analytical chemistry

Article

Cite This: Anal. Chem. 2019, 91, 3270−3276

pubs.acs.org/ac

Ultrasensitive Colorimetric Detection of Murine Norovirus Using NanoZyme Aptasensor

Pabudi Weerathunge,[†,‡] Rajesh Ramanathan,*[,†,‡] Valeria A. Torok,[§] Kate Hodgson,[§] Yun Xu,[∥,¶] Royston Goodacre,[∥,¶] Bijay Kumar Behera,[⊥] and Vipul Bansal*[,†]

[†]Ian Potter NanoBioSensing Facility, NanoBiotechnology Research Laboratory (NBRL), School of Science, RMIT University, GPO Box 2476, Melbourne, VIC 3000, Australia

[§]South Australian Research and Development Institute (SARDI), Food Safety and Innovation, GPO Box 397, Adelaide, SA 5064, Australia

[∥]School of Chemistry, Manchester Institute of Biotechnology, The University of Manchester, 131 Princess Street, Manchester M1 7DN, United Kingdom

[⊥]ICAR-Central Inland Fisheries Research Institute, Barrackpore, Kolkata 700100, India

Supporting Information

ABSTRACT: Human norovirus (NoV) remains the most common cause of viral gastroenteritis and the leading cause of viral foodborne outbreaks globally. NoV is highly pathogenic with an estimated median viral infective dose (ID_{50}) ranging from 18 to 1015 genome copies. For NoV detection, the only reliable and sensitive method available for detection and quantification is reverse transcription quantitative polymerase chain reaction (RTqPCR). NoV detection in food is particularly challenging, requiring matrix specific concentration of the virus and removal of inhibitory compounds to detection assays. Hence, the RTqPCR method poses some challenges for rapid in-field or point-of-care diagnostic applications. We propose a new colorimetric NanoZyme aptasensor strategy for rapid (10 min) and ultrasensitive (calculated Limit of Detection (LoD) of 3 viruses per assay equivalent to 30 viruses/mL of sample and experimentally demonstrated LoD of 20 viruses per assay equivalent to 200 viruses/mL) detection of the infective murine norovirus (MNV), a readily cultivable surrogate for NoV. Our approach combines the enzyme-mimic catalytic activity of gold nanoparticles with high target specificity of an MNV aptamer to create sensor probes that produce a blue color in the presence of this norovirus, such that the color intensity provides the virus concentrations. Overall, our strategy offers the most sensitive detection of norovirus or a norovirus surrogate achieved to date using a biosensor approach, enabling for the first time, the detection of MNV virion corresponding to the lower end of the ID_{50} for NoV. We further demonstrate the robustness of the norovirus NanoZyme aptasensor by testing its performance in the presence of other nontarget microorganisms, human serum and shellfish homogenate, supporting the potential of detecting norovirus in complex matrices. This new assay format can, therefore, be of significant importance as it allows ultrasensitive norovirus detection rapidly within minutes, while also offering the simplicity of use and need for nonspecialized laboratory infrastructure.

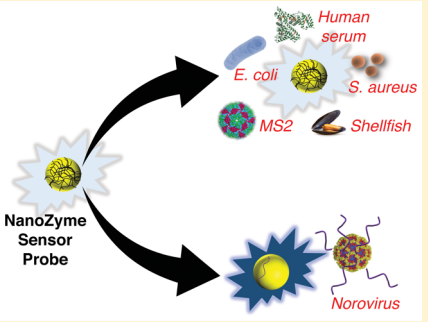

Norovirus (NoV) belongs to a genetically diverse group of small, icosahedral, nonenveloped viruses with a positive sense single-stranded RNA (ssRNA) genome.[1,2] They are the members of the family *Caliciviridae* and are the major cause of acute viral gastroenteritis worldwide, commonly known as "winter vomiting disease".[1,2] NoV is highly contagious due to its low infective dose (median infective dose, ID_{50} estimated at 18 to 1015 genome copies),[3] prolonged period of viral shedding, asymptomatic infection in some individuals, and high reoccurrence rate and high stability within the environment; posing major challenges in NoV management.[1] NoV is primarily spread through person-to-person contact, as well as, through consumption of contaminated food or water, aerosolised vomit particles or contact with contaminated surfaces. NoV is estimated to account for 267 million infections and over 200000 deaths (particularly in the young, elderly, and immunosuppressed patients) per year,[4,5] with outbreaks often occurring in semiclosed communities such as schools, nursing homes, hospitals, and cruise ships.[6] Foods can become contaminated via contact with contaminated water, poor hygiene and food handlers, with foods of highest risk being raw shellfish, berries, and ready-to-eat foods. Furthermore, the open cross-border trade policies of food products promote global outbreaks.[7−10] Collectively, these highlight the need for a rapid and accurate detection strategy for this important human and foodborne pathogen.

Received: July 24, 2018
Accepted: January 14, 2019
Published: January 14, 2019

Downloaded via UNIV OF LIVERPOOL on March 7, 2019 at 09:00:15 (UTC).
See https://pubs.acs.org/sharingguidelines for options on how to legitimately share published articles.

© 2019 American Chemical Society

DOI: 10.1021/acs.analchem.8b03300
Anal. Chem. 2019, 91, 3270−3276

Table 1. Comparison of Norovirus Detection Parameters among Various Platforms with Emphasis on Potential Viral Load (Concentrations per mL) Present in Test Analyte

detection method	target	linear dynamic range	calculated limit of detection (LoD)	signal generation time	ref
electrochemical	MNV	20−120 aM (ca. 1.2×10^4−7.2×10^4 viruses/mL)	10 aM (ca. 6000 viruses/mL)	60 min	2
commercial ELISA kit (NV-AD (III), Denka Seiken, Japan)	NoV VLP	not given	3.8 ng/mL (ca. 2.19×10^8 VLP/mL)[b]	not given	7
conventional ELISA	NoV VLP	10−10^3 ng/mL	10.4 ng/mL (ca. 6.00×10^8 VLP/mL)[b]	>12 h	7
graphene-GNP antibody ELISA	NoV VLP	10^2−10^7 pg/mL	92.7 pg/mL (*ca.* 5.35×10^6 VLP/mL)[b]	70 min	7
dot-blotting	NoV	2.7×10^6−2.7×10^8 genome copies/mL	2.7×10^6 genome copies/mL	10 min	11
microfluidics	NoV	1.6×10^5 − 7.9×10^7 genome copies/mL	9.5×10^4 genome copies/mL	60 min	69
NanoZyme aptasensor	MNV	200−10000 viruses/mL[a] OR	30 viruses/mL[a]	10 min	this work
		1320−19800 viruses/mL[a] OR	50 viruses/mL[a]		
		3300−33000 viruses/mL[a]	80 viruses/mL[a]		

[a]Linear dynamic range of the NanoZyme aptasensor is tunable by changing the sensor probe composition. [b]Calculation for conversion of protein concentration to virus-like particle (VLP) concentration is provided in Supporting Information.

The current gold standard for NoV detection and quantification is based on gene amplification techniques such as reverse transcription quantitative polymerase chain reaction (RTqPCR),[4,5] although a number of alternative methods for NoV detection have been reported (Table 1).[1,2,7,11] To our knowledge, the most sensitive alternative NoV detection system reported to date is based on an electrochemical aptasensor approach, wherein the binding of norovirus to highly specific DNA aptamers afforded a calculated limit of detection (LoD) of 180 murine norovirus (MNV) particles or 6000 MNV/mL.[2] While promising, this LoD is still far-off from meeting the lower end of the median viral infective dose (ID_{50} for NoV), estimated to range from 18 to 1015 genome copies.[3] Development of an ultrasensitive, specific, rapid, and user-friendly platform for NoV detection would be particularly advantageous for detecting clinical, environmental, and food contamination, with a possibility of portable in-field translation.

The developments in nanotechnology have seen the emergence of colorimetric and other potential biosensing platforms as a viable technology for point-of-care devices.[12−27] Gold nanoparticles (GNPs), in particular, have been at the forefront due to well-established synthesis routes, ease of surface functionalization, high stability, low cost, low toxicity and remarkable surface plasmon resonance (SPR) properties that allow a visual read-out of the sensing event.[28−38] However, GNP-based sensors that rely on color generation via the SPR properties of gold find it rather challenging to avoid aggregation in complex biological fluids, resulting in nonspecificity and false positives.[39−42] In recent years, the aggregation-induced nonspecificity of GNPs has been overcome by developing GNP-based NanoZyme sensors that do not rely upon the SPR properties, but instead take advantage of the enzyme-mimicking catalytic activity of gold nanoparticles to convert a colorless substrate into a colored product.[43−48] However, in the absence of a targeting moiety, the applicability of NanoZyme sensors remains limited, as NanoZymes can exhibit broad-spectrum catalytic activities against a range of substrates. More recently, we have been able to add an element of specificity in NanoZyme sensors by incorporating target-specific molecular recognition elements (MREs) to allow colorimetric detection of small molecules such as pesticides and antibiotics.[49,50]

The use of MREs is common in traditional biomolecular detection systems, for example, antibodies as in enzyme-linked immunosorbent assay (ELISA),[51] unique polynucleotide sequences in PCR,[52] or lectins in lectin-binding assays (LBA).[53] A relatively new class of nonstereotypical MRE that has remarkable potential in providing specificity to biosensors are aptamers.[16,54] These synthetic nucleic acids fold into unique three-dimensional conformations and are capable of binding to their targets with high specificity and outstanding affinity.[16,55] The distinguishing feature of aptamers from other MREs is that they can be raised in silico against the vast majority of targets ranging from small molecules[49,50] to complex biological entities such as cancer cells,[56,57] pathogenic bacteria,[58,59] and viruses.[2,60] Aptamers are particularly attractive for biosensors development as they also exhibit high ambient storage stability and affordable ongoing in vitro synthesis cost once the aptamers have been designed for a particular assay.[16,55,61]

In the current study, we combine the outstanding target-specificity of a MNV *AG3* aptamer[2] with the NanoZyme activity of GNPs to develop a rapid colorimetric sensor for ultrasensitive and highly specific detection of the MNV virion. The two reasons for using MNV instead of human norovirus (NoVs) are (i) the production of NoV involves a laborious process[62] and (ii) MNV is an infectious easily cultivable NoV surrogate enabling the infective particles to be accurately quantified using a plaque assay. Such a model allows the developed sensor to be evaluated for accuracy in detecting infective virus particles as opposed to noninfective coat protein or nonencapsidated/damaged viral genome. Neither virus-like particles (VLPs) or NoV strains sourced from human faeces accurately allow for this as quantification is based on total protein concentration or detection of both infective and noninfective viral genomes, respectively. Therefore, the current work utilizes MNV, a cultivable surrogate of NoV as a model system, and demonstrates that the proposed NanoZyme aptasensor technology can detect the infective MNV with a calculated LoD of just three viruses in 100 μL of sample (equivalent to 30 viruses/mL), the lowest known limit, achieved to date, and that too within a short assay time of

DOI: 10.1021/acs.analchem.8b03300
Anal. Chem. 2019, 91, 3270−3276

Scheme 1. Working Principle of the Norovirus NanoZyme Aptasensor; Schematic Illustration Outlining the Steps Involved during Norovirus Sensing[a]

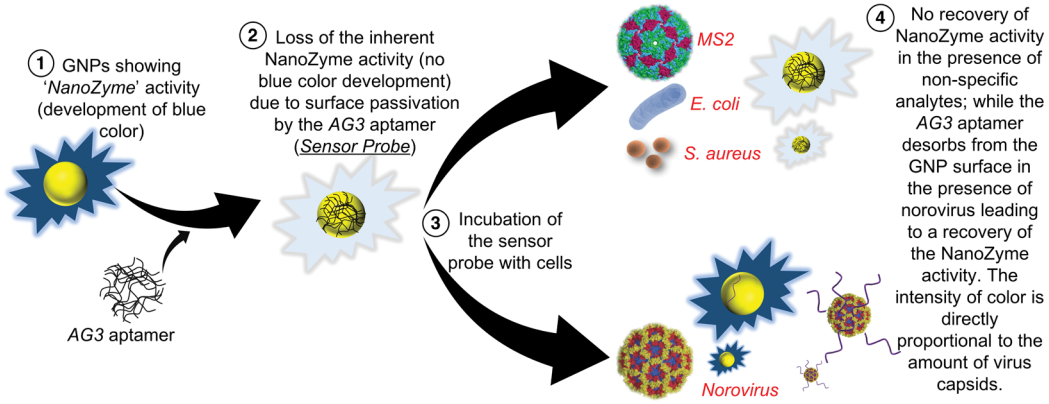

[a]Step 1 shows the NanoZyme activity of GNPs that converts a colorless TMB substrate to a blue oxidized product. Step 2 involves the noncovalent adsorption of the MNV-specific *AG3* aptamer molecules on to the surface of GNPs, leading to the loss of the inherent NanoZyme activity. This GNP-aptamer conjugate serves as the "*Sensor Probe*". Step 3 involves the incubation of the sensor probe with different cells, including murine norovirus (specific target), *MS2* phage (structurally similar to norovirus), *S. aureus* and *E. coli*. Step 4 shows that in the presence of norovirus, the aptamers desorb from the surface of the GNPs leading to the recovery of the NanoZyme activity, producing a blue color. The intensity of color will be proportional to the amount of norovirus present in the sample. In contrast, since aptamers will not have any affinity to other contaminants, no recovery of the NanoZyme activity will be observed, thereby resulting in no color in the presence of nonspecific targets.

only 10 min. We further demonstrate the potential applicability of our Nanozyme aptasensor in the real-world scenario by demonstrating that it retains its functionality in the presence of potential contaminants such as other bacteria and viruses while being able to reliably detect MNV in complex matrices of human serum and shellfish homogenate. These outcomes offer new opportunities for practical deployment of the norovirus NanoZyme aptasensor for detecting human infections as well as contaminated food.

Scheme 1 illustrates the NanoZyme aptasensor approach for colorimetric detection of norovirus, providing an ultrasensitive and highly specific visual readout of the sensing event within 10 min. The underlying concept is built around utilizing the inherent peroxidase-like NanoZyme activity of GNPs to generate a characteristic blue color through the oxidation of a colorless peroxidase substrate TMB (3,3′,5,5′-tetramethylbenzidine) (Step 1). Surface passivation of the GNPs with a MNV capsid-specific *AG3* aptamer[2] results in the loss of the color-generating NanoZyme activity (Step 2). This GNP-aptamer nanoconjugate serves as the sensor probe. When this sensor probe is exposed to the analyte (Step 3), the NanoZyme activity toward generating blue color via TMB oxidation is selectively recovered in the presence of norovirus and not in the presence of any other nonspecific virus or bacterial cell (Step 4). The recovery of the NanoZyme activity in the presence of norovirus is due to the high affinity of *AG3* aptamer toward MNV, which causes conformational changes in the aptamer in the presence of norovirus, leading to their displacement from the GNP surface and binding to the MNV capsid. This aptamer desorption exposes the catalytic sites on the surface of the GNPs to allow TMB oxidation into a blue product. In contrast, in the absence of norovirus, but in the presence of nonspecific targets such as Gram-positive bacteria *Staphylococcus aureus*, Gram-negative bacteria *Escherichia coli*, or even a structurally similar virus, such as *E. coli* bacteriophage MS2 (MS2 phage), the aptamers do not desorb from the GNP surface and the NanoZyme activity is not recovered, thereby offering selectivity to the sensor.

As the generation of blue color due to the NanoZyme activity of GNPs is central to the sensor mechanism, we first established the enzyme-like characteristics of tyrosine-functionalized GNPs (detailed in Supporting Information, Figures S1–S4) synthesized using a previously established protocol (Figure S1). The GNPs were of low polydispersity, high crystallinity, and of quasi-spherical morphology, with an average diameter of about 20 nm (Figure S2). The peroxidase-mimic NanoZyme activity of these GNPs shows a nanoparticle, TMB, and H_2O_2 concentration-dependent increase in activity (Figure S3), as observed for other NanoZymes.[12,45,46,49,50,63,64] We also calculated the kinetic parameters such as Michaelis–Menten constant (K_m), maximum initial velocity (V_{max}), and turnover number (K_{cat}) for the NanoZyme-driven reactions (Table S1 and Figure S4). The NanoZyme kinetic parameters suggest that tyrosine-functionalized GNPs offer over 3 orders of magnitude higher affinity to colorigenic TMB substrate in comparison to that to the co-substrate H_2O_2. This is a desirable property in terms of achieving high sensitivity and reproducibility during sensing, as high affinity of NanoZyme toward TMB is likely to allow even low concentrations of target analyte to be identified while using the sensor probe developed in the next stage.

We then developed the sensor probe through binding of MNV-specific *AG3* aptamer to the surface of GNPs. This required determination of the minimum concentration of the *AG3* aptamer needed to passivate the GNP surface without the availability of excessive amounts of free aptamer molecules around the GNP-aptamer nanoconjugates. Figure 1 shows that the NanoZyme activity of GNPs decreases with the increasing aptamer concentration, as structural flexibility of aptamers allows them to passivate the GNP surface via electrostatic interactions.[65] As such, our calculations reveal that an optimum sensor probe requires an average of ∼250 aptamer molecules per GNP to block its NanoZyme activity (see Supporting Information for details). The nonlinear least-square fitting of the aptamer-GNP interactions revealed a dissociation constant (K_d) of 1.85×10^{-8} M and a Hill coefficient

DOI: 10.1021/acs.analchem.8b03300
Anal. Chem. 2019, 91, 3270–3276

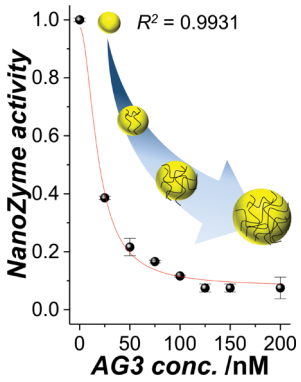

Figure 1. Sensor probe fabrication. Decrease in the NanoZyme activity of the GNPs plotted as a function of *AG3* aptamer concentration. The data were fitted (red curve) using a nonlinear least-squares reverse Hill equation.

(association stoichiometry) of 1.91. The Hill coefficient value of >1 reflects a positive cooperative binding behavior, such that the binding of an aptamer molecule to the GNP surface enhances the affinity of other aptamer molecules to bind to the surface of the NanoZyme (Table S2).[66,67] The observed K_d for the aptamer−GNP interactions corroborates well with the previously observed values for stable noncovalently bonded biomolecule−GNP systems.[68] The previous work has shown that the K_d for the *AG3* aptamer to MNV is in the low picomolar range (10^{-12} M). Conversely, our current work shows the K_d for the *AG3* aptamer to the GNPs is 1.85×10^{-8} M. This suggests that the *AG3* aptamer has almost 4 orders of magnitude higher binding affinity to MNV than to the GNP. This relative interaction strength of the *AG3* aptamer to MNV versus GNP suggests that when the GNP−aptamer conjugate is exposed to MNV (Step 3, Scheme 1), the aptamers will dissociate from the surface of the GNPs to bind effectively to the target norovirus (Step 4, Scheme 1). Furthermore, the GNP−aptamer nanoconjugates remain stable in solution post aptamer functionalization (Figure S5, Supporting Information) and serve as sensor probes for subsequent colorimetric detection of norovirus.

The utility of these NanoZyme aptasensor probes for rapid, sensitive, and selective detection of norovirus was assessed by first incubating the sensor probe independently with increasing population of different viruses and bacteria for 10 min. We selected three different biological backgrounds in addition to norovirus, each representing a specific group of microorganisms that may be present as cross-contaminants in the analyte sample containing norovirus. Among these, MNV serves as the target of interest, MS2 phage represents a nontarget virus with morphological and surface characteristics resembling noroviruses, *Staphylococcus aureus* represents Gram-positive group of bacteria, and *Escherichia coli* represents Gram-negative bacteria (cell preparation outlined in Supporting Information). Figure 2a shows the colorimetric response corresponding to each biological background obtained from the sensor probe in 10 min. It is clear that the NanoZyme activity is recovered specifically in the presence of norovirus, while all other microorganisms, including structurally similar MS2 phage, show only basal level activity. This highly specific response is attributed to the high affinity of *AG3* aptamers that were specifically raised against the MNV surface. Furthermore, the sensor response (i.e., the intensity of blue color) increases with the corresponding increase in the number of MNVs, supporting the viability of the proposed approach for norovirus sensing. As such, this norovirus NanoZyme aptasensor shows an outstanding sensitivity along with an impressive linear operating dynamic range of 20−1000 norovirus detection with high reliability (R^2 = 0.9987) and that too within an assay time of just 10 min.

To understand the underlying factors for this ultrasensitive response, we further calculated the absolute velocity of the sensor probe-induced reaction in the absence and presence of MNVs at the sensing time-point (t = 10 min). Figures 2b and S6 show that the absolute velocity of the reaction increases linearly with increasing MNV concentration. Remarkably, a 63% increase in the velocity is observed in the presence of as low as 20 MNVs, while 1000 MNVs enhances the TMB oxidation rate by 10.8×. The calculated limit of detection (LoD) for this assay is 3 MNV, which will correspond to 37% higher reaction velocity relative to that of the sensor probe (based on the regression analysis in Figure S6). While the current study shows that we can reliably detect 20 MNV

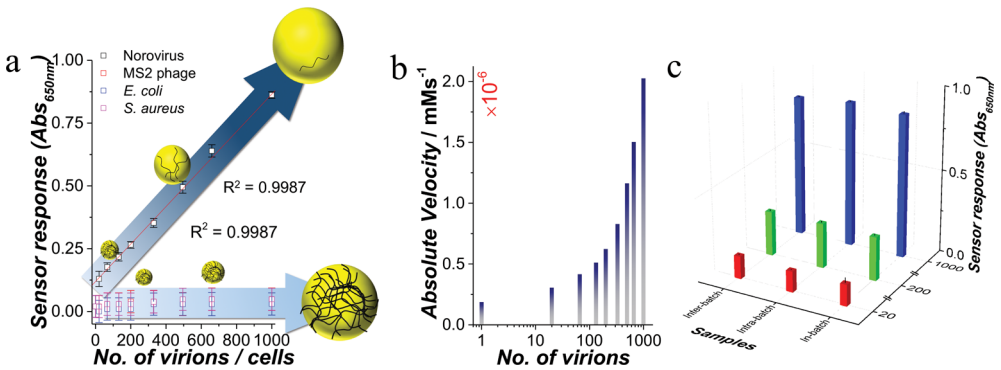

Figure 2. Sensor response for norovirus detection. (a) Colorimetric sensor response obtained from the incubation of the sensor probe for 10 min with increasing number of different biological entities including MNV, MS2 phage, *S. aureus*, and *E. coli*. The arrows represent the change in the intensity of blue color formed as a result of aptamer dissociation from the GNP surface leading to the recovery of the NanoZyme activity. The red curve shows the linear fit of the sensor response in the presence of increasing number of norovirus. (b) The reaction velocity calculated from the sensor response using enzyme kinetic theory in the absence and presence of increasing number of norovirus. (c) In-batch, intra-batch and inter-batch sensor reproducibility for three independent amounts of norovirus (20, 200, and 1000) with corresponding precision and accuracy outlined in Table S3, Supporting Information.

DOI: 10.1021/acs.analchem.8b03300
Anal. Chem. 2019, 91, 3270−3276

experimentally, it is also likely that we can experimentally detect the LoD of 3 MNV through employing robotic systems that can circumvent potential human sampling errors. Furthermore, considering that our assay employs 100 μL of the original viral sample in a total assay volume of 200 μL, we have experimentally shown that the current NanoZyme aptasensor can reliably detect at least 200 MNV/mL of the original sample. Considering the LoD of 3 MNV per assay, it should therefore be possible to detect a norovirus concentration of 30 MNV/mL in the original sample. This sensitivity is within the estimated median ID_{50} of NoV (18−1015 viral genome copies).[3]

Another desirable feature in a sensor is the ability to operate across a large range of target concentrations. However, this remains challenging as beyond a certain target concentration, the sensor response starts to saturate, underestimating the target concentration. We also noticed this limitation in our NanoZyme aptasensor, such that beyond 1000 MNVs in the assay, the sensor response became nonlinear with respect to the number of virions. To overcome this issue, we investigated the possibility of active modulation of the dynamic operational range of the norovirus NanoZyme aptasensor by changing the concentration of the NanoZyme (GNPs) in our sensor probe. When the concentration of GNPs during GNP-aptamer sensor probe fabrication was changed from 75 μM originally to 100 μM and 150 μM; the linear dynamic range of operation could be actively modulated from 20−1000 MNV originally to 132−1980 and 330−3300 MNV, respectively (Figure S7, Supporting Information). While the norovirus sensors with low detection limits are more desirable, the ability of the NanoZyme sensor to operate in different dynamic ranges will offer design flexibility for future in-field applications.

We further assessed the precision and accuracy of the norovirus sensor operating in the linear dynamic range of 20−1000 MNV under different conditions at the viral loads of 20, 200, and 1000 MNV per assay (Figure 2c). The first test involved performing 20 repeat experiments using sensor probes prepared in a single batch (in-batch). Subsequently, intra-batch variations (i.e., creating the sensor probe on different days using the GNPs prepared in a single batch) and inter-batch variations (i.e., creating the sensor probe using two independently synthesized GNPs) in norovirus sensor response were assessed. In each of these cases, the sensor responded with >95% (95.9−99.3%) precision, >95% (95−100%) accuracy at a significance level of 0.05, and 100% accuracy at a significance level of 0.1 (see Table S3, Supporting Information). These observations support the robustness of the NanoZyme aptasensor. The unprecedented sensitivity of the current norovirus sensing platform over previously reported norovirus sensors is summarized in Table 1. To allow a valid comparison between different norovirus sensors, the sensor performance data presented in Table 1 have been normalized to virus per mL of the original sample containing norovirus. The most sensitive norovirus detection system reported to date is based on an electrochemical aptasensor that offers a linear dynamic range of 360−2170 MNV (equivalent of 12000−72333 MNV/mL) with a LoD of 6000 MNV/mL.[2] In comparison, our current sensor shows 200× higher sensitivity with an absolute LoD of ∼3 viruses (30 MNV/mL) along with a tunable linear dynamic detection range that allows detection of 20−3300 norovirus during the assay, facilitating the viral loads of 200−33000 norovirus/mL detectable in test analyte. This outlines the outstanding sensitivity and robustness of the current NanoZyme aptasensor technology to selectively detect norovirus. In addition, the simplicity of the current assay and eliminating the need for trained technical personnel can potentially offer a viable option to develop point-of-care norovirus detection devices.

We further evaluated the target-specific performance of the norovirus NanoZyme aptasensor in conditions similar to those encountered during the real-world analysis of a potentially contaminated sample (Figure 3 and Table S4). These included

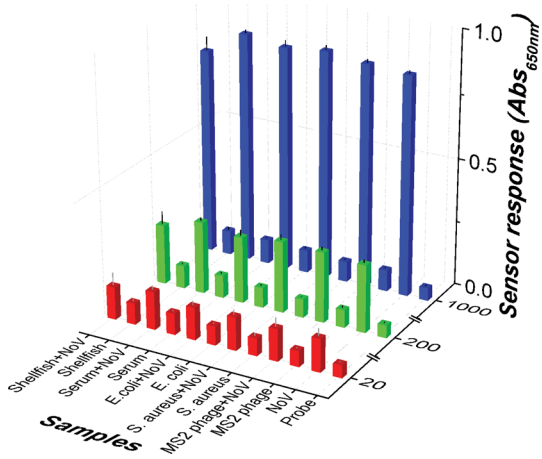

Figure 3. Performance of the NanoZyme aptasensor in complex matrices mimicking the real-world scenario. Sensor response obtained for three independent amounts of norovirus (20, 200, and 1000) as well as in the absence of norovirus; in the presence of a higher population (100000 cells) of nonspecific targets (MS2 phage, *S. aureus*, and *E. coli*); in human serum; and in the shellfish (mussel) homogenate.

three different scenarios, the first mimicking a situation where nonspecific bacterial and viral loads might be significantly higher (10^5) than norovirus (20, 200, and 1000); the second case considering the potential interference caused by exogenous proteins (human sera); and the third scenario testing the ability of norovirus detection in raw shellfish (mussels) homogenate. The contaminant species present in these scenarios may potentially lead to non-specific response due to sample matrix interference. However, the robustness of the NanoZyme aptasensor supported by the high affinity of *AG3* aptamer toward MNV resulted in excellent recoveries ranging between 96.7 and 101.8% during norovirus detection in each of these cases, as determined using the linear fit model obtained from Figure 2b (Table 2). This demonstrates the outstanding ability of the current NanoZyme aptasensor technology to selectively detect norovirus even in the presence of other viral and bacterial contaminants, as well as in complex biological matrices.

In summary, we have demonstrated a highly robust NanoZyme aptasensor technology for rapid, highly selective and ultrasensitive colorimetric detection of MNV, a cultivable surrogate of human NoV. The proposed sensing technology combines the outstanding affinity of specific aptamers with the inherent peroxidase-like NanoZyme activity of GNPs to develop a robust platform for norovirus sensing with potential for further point-of-care human diagnostic and in-field food and environmental screening development. This novel technology is the most sensitive norovirus sensor reported to date, which for the first time, demonstrates the ability to detect

DOI: 10.1021/acs.analchem.8b03300
Anal. Chem. 2019, 91, 3270−3276

Table 2. Norovirus Recovery Obtained from the NanoZyme Aptasensor in the Presence of Different Contaminants

contaminant	actual number of norovirus	recovery[a] (%)
MS2 phage	20	99.6
	200	100.9
	1000	100.6
S. aureus	20	99.8
	200	101.2
	1000	101.7
E. coli	20	99.8
	200	99.6
	1000	100.8
human serum	20	101.8
	200	101.3
	1000	102
shellfish	20	96.7
	200	97.4
	1000	96.8

[a]100% recovery corresponds to expected norovirus numbers, whereas shifts toward lower/higher values represent relative underestimation/overestimation of viral loads during norovirus quantification.

virus corresponding to a low infective dose. The potential of this colorimetric technology in eliminating the need for expensive instrumentation and trained specialized technical personnel may allow in-field translation as a point-of-care NoV diagnostic device.

■ ASSOCIATED CONTENT

Supporting Information

The Supporting Information is available free of charge on the ACS Publications website at DOI: 10.1021/acs.analchem.8b03300.

Details of chemicals, experiments, instruments, materials characterization, and sensor performance evaluation (PDF).

■ AUTHOR INFORMATION

Corresponding Authors

*E-mail: rajesh.ramanathan@rmit.edu.au.
*E-mail: vipul.bansal@rmit.edu.au.

ORCID

Rajesh Ramanathan: 0000-0002-8500-9148
Royston Goodacre: 0000-0003-2230-645X
Vipul Bansal: 0000-0002-3354-4317

Present Address

¶(R.G. and Y.X.) Department of Biochemistry, Institute of Integrative Biology, University of Liverpool, Biosciences Building, Crown Street, Liverpool L69 7ZB, United Kingdom

Author Contributions

‡These authors contributed equally. The manuscript was written through contributions of all authors.

Notes

The authors declare no competing financial interest.

■ ACKNOWLEDGMENTS

This work was supported through an Australian Research Council (ARC) Future Fellowship to V.B. (FT140101285). V.B. and R.R. acknowledge the ARC for funding support through the ARC Discovery scheme (DP170103477). R.R. acknowledges RMIT University for the Vice Chancellor Fellowship. B.K.B. thanks the Commonwealth of Australia for an Endeavour Research Fellowship. The authors acknowledge the generous support of the Ian Potter Foundation for establishing Sir Ian Potter NanoBioSensing Facility at RMIT University. The authors also acknowledge the support from the RMIT Microscopy and Microanalysis Facility (RMMF) for technical assistance and providing access to characterization facilities. Support from the Australian Seafood CRC and Fisheries Research and Development Corporation are also acknowledged (FRDC 2011/726).

■ REFERENCES

(1) Patel, M. M.; Hall, A. J.; Vinjé, J.; Parashar, U. D. *J. Clin. Virol.* **2009**, *44*, 1−8.
(2) Giamberardino, A.; Labib, M.; Hassan, E. M.; Tetro, J. A.; Springthorpe, S.; Sattar, S. A.; Berezovski, M. V.; DeRosa, M. C. *PLoS One* **2013**, *8*, e79087.
(3) Teunis, P. F. M.; Moe, C. L.; Liu, P.; E. Miller, S.; Lindesmith, L.; Baric, R. S.; Le Pendu, J.; Calderon, R. L. *J. Med. Virol.* **2008**, *80*, 1468−1476.
(4) Lopman, B.; Atmar, R.; Baric, R.; Estes, M.; Hall, A.; Iturriza-Gómara, M.; Kang, C.; Lee, B.; Parashar, U.; Riddle, M.; Vinjé, J. Global burden of norovirus and prospects for vaccine development; *CDC Foundation Global Burden Report*; CDC, 2015; pp 1−44.
(5) Lopman, B. A.; Steele, D.; Kirkwood, C. D.; Parashar, U. D. *PLoS Med.* **2016**, *13*, e1001999.
(6) Debbink, K.; Lindesmith, L. C.; Donaldson, E. F.; Baric, R. S. *PLoS Pathog.* **2012**, *8*, e1002921.
(7) Ahmed, S. R.; Takemeura, K.; Li, T.-C.; Kitamoto, N.; Tanaka, T.; Suzuki, T.; Park, E. Y. *Biosens. Bioelectron.* **2017**, *87*, 558−565.
(8) Hagström, A. E.; Garvey, G.; Paterson, A. S.; Dhamane, S.; Adhikari, M.; Estes, M. K.; Strych, U.; Kourentzi, K.; Atmar, R. L.; Willson, R. C. *PLoS One* **2015**, *10*, e0126571.
(9) Gould, L. H.; Kline, J.; Monahan, C.; Vierk, K. *Emerging Infect. Dis.* **2017**, *23*, 525−528.
(10) Holley, R. A. *Compr. Rev. Food Sci. Food Saf.* **2011**, *10*, 131−142.
(11) Kim, J.-H.; Park, J.-E.; Lin, M.; Kim, S.; Kim, G.-H.; Park, S.; Ko, G.; Nam, J.-M. *Adv. Mater.* **2017**, *29*, 1702945.
(12) Karim, M. N.; Anderson, S. R.; Singh, S.; Ramanathan, R.; Bansal, V. *Biosens. Bioelectron.* **2018**, *110*, 8−15.
(13) Daniel, M. C.; Astruc, D. *Chem. Rev.* **2004**, *104*, 293−346.
(14) Saha, K.; Agasti, S. S.; Kim, C.; Li, X.; Rotello, V. M. *Chem. Rev.* **2012**, *112*, 2739−2779.
(15) Miranda, O. R.; Creran, B.; Rotello, V. M. *Curr. Opin. Chem. Biol.* **2010**, *14*, 728−736.
(16) Sharma, T. K.; Ramanathan, R.; Rakwal, R.; Agrawal, G. K.; Bansal, V. *Proteomics* **2015**, *15*, 1680−1692.
(17) Walia, S.; Sabri, Y.; Ahmed, T.; Field, M. R.; Ramanathan, R.; Arash, A.; Bhargava, S. K.; Sriram, S.; Bhaskaran, M.; Bansal, V. *2D Mater.* **2017**, *4*, 015025.
(18) Ramanathan, R.; Walia, S.; Kandjani, A. E.; Balendran, S.; Mohammadtaheri, M.; Bhargava, S. K.; Kalantar-zadeh, K.; Bansal, V. *Langmuir* **2015**, *31*, 1581−1587.
(19) Ramanathan, R.; Kandjani, A. E.; Walia, S.; Balendhran, S.; Bhargava, S. K.; Kalantar-zadeh, K.; Bansal, V. *RSC Adv.* **2013**, *3*, 17654−17658.
(20) De La Rica, R.; Stevens, M. M. *Nat. Nanotechnol.* **2012**, *7*, 821.
(21) Rodríguez-Lorenzo, L.; De La Rica, R.; Álvarez-Puebla, R. A.; Liz-Marzán, L. M.; Stevens, M. M. *Nat. Mater.* **2012**, *11*, 604.
(22) Le, N. D. B.; Yesilbag Tonga, G.; Mout, R.; Kim, S.-T.; Wille, M. E.; Rana, S.; Dunphy, K. A.; Jerry, D. J.; Yazdani, M.; Ramanathan, R.; Rotello, C. M.; Rotello, V. M. *J. Am. Chem. Soc.* **2017**, *139*, 8008−8012.
(23) Rezk, A. R.; Walia, S.; Ramanathan, R.; Nili, H.; Ou, J. Z.; Bansal, V.; Friend, J. R.; Bhaskaran, M.; Yeo, L. Y.; Sriram, S. *Adv. Opt. Mater.* **2015**, *3*, 888−894.

DOI: 10.1021/acs.analchem.8b03300
Anal. Chem. 2019, 91, 3270−3276

(24) Behera, B. K.; Das, A.; Sarkar, D. J.; Weerathunge, P.; Parida, P. K.; Das, B. K.; Thavamani, P.; Ramanathan, R.; Bansal, V. *Environ. Pollut.* **2018**, *241*, 212−233.
(25) Zou, W.; González, A.; Jampaiah, D.; Ramanathan, R.; Taha, M.; Walia, S.; Sriram, S.; Bhaskaran, M.; Dominguez-Vera, J. M.; Bansal, V. *Nat. Commun.* **2018**, *9*, 3743.
(26) Selvakannan, P.; Ramanathan, R.; Plowman, B. J.; Sabri, Y. M.; Daima, H. K.; O'Mullane, A. P.; Bansal, V.; Bhargava, S. K. *Phys. Chem. Chem. Phys.* **2013**, *15*, 12920−12929.
(27) Chen, F.; Tang, F.; Yang, C.-T.; Zhao, X.; Wang, J.; Thierry, B.; Bansal, V.; Dai, J.; Zhou, X. *ACS Sens.* **2018**, *3*, 2175.
(28) Muhamadali, H.; Subaihi, A.; Mohammadtaheri, M.; Xu, Y.; Ellis, D. I.; Ramanathan, R.; Bansal, V.; Goodacre, R. *Analyst* **2016**, *141*, 5127−5136.
(29) Boisselier, E.; Astruc, D. *Chem. Soc. Rev.* **2009**, *38*, 1759−1782.
(30) Zohora, N.; Kumar, D.; Yazdani, M.; Rotello, V. M.; Ramanathan, R.; Bansal, V. *Colloids Surf., A* **2017**, *532*, 451−457.
(31) Zayats, M.; Baron, R.; Popov, I.; Willner, I. *Nano Lett.* **2005**, *5*, 21−25.
(32) Carnovale, C.; Bryant, G.; Shukla, R.; Bansal, V. *Prog. Mater. Sci.* **2016**, *83*, 152−190.
(33) Sabri, Y. M.; Ippolito, S. J.; Tardio, J.; Bansal, V.; O'Mullane, A. P.; Bhargava, S. K. *Sci. Rep.* **2015**, *4*, 6741.
(34) Kim, J. E.; Choi, J. H.; Colas, M.; Kim, D. H.; Lee, H. *Biosens. Bioelectron.* **2016**, *80*, 543−559.
(35) Mohammadzadeh-Asl, S.; Keshtkar, A.; Ezzati Nazhad Dolatabadi, J.; de la Guardia, M. *Biosens. Bioelectron.* **2018**, *110*, 118−131.
(36) Syedmoradi, L.; Daneshpour, M.; Alvandipour, M.; Gomez, F. A.; Hajghassem, H.; Omidfar, K. *Biosens. Bioelectron.* **2017**, *87*, 373−387.
(37) Reguera, J.; Langer, J.; Jiménez De Aberasturi, D.; Liz-Marzán, L. M. *Chem. Soc. Rev.* **2017**, *46*, 3866−3885.
(38) Anderson, S. R.; Mohammadtaheri, M.; Kumar, D.; O'Mullane, A. P.; Field, M. R.; Ramanathan, R.; Bansal, V. *Adv. Mater. Interfaces* **2016**, *3*, 1500632.
(39) Vilela, D.; González, M. C.; Escarpa, A. *Anal. Chim. Acta* **2012**, *751*, 24−43.
(40) Jv, Y.; Li, B.; Cao, R. *Chem. Commun.* **2010**, *46*, 8017−8019.
(41) Long, Y. J.; Li, Y. F.; Liu, Y.; Zheng, J. J.; Tang, J.; Huang, C. Z. *Chem. Commun.* **2011**, *47*, 11939−11941.
(42) Guo, L.; Xu, Y.; Ferhan, A. R.; Chen, G.; Kim, D.-H. *J. Am. Chem. Soc.* **2013**, *135*, 12338−12345.
(43) Lin, Y.; Ren, J.; Qu, X. *Acc. Chem. Res.* **2014**, *47*, 1097−1105.
(44) Weerathunge, P.; Sharma, T. K.; Ramanathan, R.; Bansal, V. Nanozyme-Based Environmental Monitoring. *Advanced Environmental Analysis: Applications of Nanomaterials*; The Royal Society of Chemistry, 2017; Vol. 2, pp 108−132.
(45) Wei, H.; Wang, E. *Chem. Soc. Rev.* **2013**, *42*, 6060−6093.
(46) Wang, X.; Hu, Y.; Wei, H. *Inorg. Chem. Front.* **2016**, *3*, 41−60.
(47) Tonga, G. Y.; Jeong, Y.; Duncan, B.; Mizuhara, T.; Mout, R.; Das, R.; Kim, S. T.; Yeh, Y.-C.; Yan, B.; Hou, S.; Rotello, V. M. *Nat. Chem.* **2015**, *7*, 597−603.
(48) de la Rica, R.; Stevens, M. M. *Nat. Nanotechnol.* **2012**, *7*, 821−824.
(49) Weerathunge, P.; Ramanathan, R.; Shukla, R.; Sharma, T. K.; Bansal, V. *Anal. Chem.* **2014**, *86*, 11937−11941.
(50) Sharma, T. K.; Ramanathan, R.; Weerathunge, P.; Mohammadtaheri, M.; Daima, H. K.; Shukla, R.; Bansal, V. *Chem. Commun.* **2014**, *50*, 15856−15859.
(51) Byrne, B.; Stack, E.; Gilmartin, N.; O'Kennedy, R. *Sensors* **2009**, *9*, 4407−4445.
(52) Kovárová, M.; Dráber, P. *Nucleic Acids Res.* **2000**, *28*, e70−e70.
(53) Zhao, J.; Patwa, T. H.; Qiu, W.; Shedden, K.; Hinderer, R.; Misek, D. E.; Anderson, M. A.; Simeone, D. M.; Lubman, D. M. *J. Proteome Res.* **2007**, *6*, 1864−1874.
(54) Dhiman, A.; Kalra, P.; Bansal, V.; Bruno, J. G.; Sharma, T. K. *Sens. Actuators, B* **2017**, *246*, 535−553.
(55) Keefe, A. D.; Pai, S.; Ellington, A. *Nat. Rev. Drug Discovery* **2010**, *9*, 537−550.
(56) Hung, L.-Y.; Wang, C.-H.; Che, Y.-J.; Fu, C.-Y.; Chang, H.-Y.; Wang, K.; Lee, G.-B. *Sci. Rep.* **2015**, *5*, na.
(57) Wu, X.; Chen, J.; Wu, M.; Zhao, J. X. *Theranostics* **2015**, *5*, 322.
(58) Chang, Y.-C.; Yang, C.-Y.; Sun, R.-L.; Cheng, Y.-F.; Kao, W.-C.; Yang, P.-C. *Sci. Rep.* **2013**, *3*, 1863.
(59) Yang, M.; Peng, Z.; Ning, Y.; Chen, Y.; Zhou, Q.; Deng, L. *Sensors* **2013**, *13*, 6865−6881.
(60) Park, J.-W.; Lee, S. J.; Choi, E.-J.; Kim, J.; Song, J.-Y.; Gu, M. B. *Biosens. Bioelectron.* **2014**, *51*, 324−329.
(61) Ruscito, A.; DeRosa, M. C. *Front. Chem.* **2016**, *4*, na.
(62) Ettayebi, K.; Crawford, S. E.; Murakami, K.; Broughman, J. R.; Karandikar, U.; Tenge, V. R.; Neill, F. H.; Blutt, S. E.; Zeng, X.-L.; Qu, L.; Kou, B.; Opekun, A. R.; Burrin, D.; Graham, D. Y.; Ramani, S.; Atmar, R. L.; Estes, M. K. *Science* **2016**, *353*, 1387−1393.
(63) Singh, M.; Weerathunge, P.; Liyanage, P. D.; Mayes, E.; Ramanathan, R.; Bansal, V. *Langmuir* **2017**, *33*, 10006−10015.
(64) Karim, M. N.; Singh, M.; Weerathunge, P.; Bian, P.; Zheng, R.; Dekiwadia, C.; Ahmed, T.; Walia, S.; Della Gaspera, E.; Singh, S.; Ramanathan, R.; Bansal, V. *ACS Appl. Nano Mater.* **2018**, *1*, 1694−1704.
(65) Li, H.; Rothberg, L. *Proc. Natl. Acad. Sci. U. S. A.* **2004**, *101*, 14036−14039.
(66) Hulme, E. C.; Trevethick, M. A. *Br. J. Pharmacol.* **2010**, *161*, 1219−1237.
(67) Dahan, D. S.; Dibas, M. I.; Petersson, E. J.; Auyeung, V. C.; Chanda, B.; Bezanilla, F.; Dougherty, D. A.; Lester, H. A. *Proc. Natl. Acad. Sci. U. S. A.* **2004**, *101*, 10195−10200.
(68) Rana, S.; Le, N. D. B.; Mout, R.; Saha, K.; Gulen, Y. T.; Bain, R. E. S.; Miranda, O. R.; Rotello, C. M.; Rotello, V. M. *Nat. Nanotechnol.* **2015**, *10*, 65−69.
(69) Han, K. N.; Choi, J.-S.; Kwon, J. *Sci. Rep.* **2016**, *6*, 25710.

DOI: 10.1021/acs.analchem.8b03300
Anal. Chem. 2019, 91, 3270−3276